SJESR: Vol. 2, No. 4, 2024, 95-113

SAMARRA JOURNAL OF ENGINEERING SCIENCE AND RESEARCH

Settlement of Circular Footing under Earthquake Load in Sandy Soil Treated with Steel Slag

Ahmed H. Hussein

Department of Civil Engineering, College of Engineering, University of Samarra, Iraq

Keywords

Settlement, Earthquake, Steel slag, Sandy soil.

Corresponding Author

E-mail: ahmed.hammad@uosamarra.edu.iq

Abstract

This research studies the effect of treating sandy soil with steel slag under seismic action (El Centro, Kobe) because of the present increase in seismic effectiveness and going to minimize damage of the foundations by excessive settlement. Steel slag was added to sandy soil with three percentages (3%, 6%, and 9%) and compacted with a relative density of 56%, and 77%. The prepared soil samples were tested on a shaking table (vibrating table). Settlement occurs due to dynamic force. A circular foundation with a diameter of 100 mm and a thickness of 40 mm was used, and the applied load was constant at 3.81kg. When the earthquake accelerates more, it results in increased settlement of the circular foundation based on sandy soil, in a dry or saturated state. The settlement of the foundation increases when subjected to the El Centro and Kobe earthquakes. In addition, increasing the mixing ratios and relative density decreases the settlement of the foundation subjected to earthquake. As the mixing ratio increased to 9%, the settlement ratio decreased. In the dry state, the settlement decreased by (37.42% and 36.77%) at a relative density of 56% for the El Centro and Kobe respectively. At a relative density of 77%, the settlement rate decreased by (39.31% and 39.89%), respectively. In the saturated state, the settlement decreased by (28.05% and 22.92%) at a relative density of 56% for the El Centro and Kobe respectively. At a relative density of 77%, the settlement rate decreased by (31.87% and 25.17%) for the El Centro and Kobe respectively. The settlement for the saturated state was twice that for the dry state.

1. Introduction:

Civil engineers are diligently looking for novel alternative materials to meet the need for cost-effective solutions in ground improvement and maintaining limited natural resources. Additionally, there is a limitation on constructing new quarries due to environmental worries. Hence, an increasing demand for something that may partially replace sand while offering enhanced characteristics. Within this particular framework, the utilization of steel slag, a byproduct of steel production, shows potential as a viable substitute material that may be combined with sand. Steel slag is a byproduct produced in a steel furnace and used in various construction applications [11].

Recycling and reusing steel slag has become more appealing than disposing of it. The conversion of iron to steel produces steel slag, one of the industrial byproducts still disposed of in landfills. In steel-making furnaces, impurities are removed from molten steel. A slag is a molten liquid of complex silicates and oxides which solidifies when cooled. Wray and Meyer [13] calculated that 50 million metric tons of steel slag were produced worldwide in 2002. The building industry has developed the utilization of steel slag in several applications. Slag has a substantial load-bearing capacity and exceptional resistance to wear, making it suitable for use as a cement and road-based material for courses [6]. Including coarse and fine aggregate in a cement-concrete mixture enhances the strength of poor soil by increasing the internal friction angle and particle density, as demonstrated by [11].

Indraratna [7] establishes that milled slag is most efficient in enhancing the internal friction angle of the studied colluvial soil. Yadu and Tripathi [14] studied the capacity of combining granulated blast furnace slag (GBS) with fly ash to turn into unstable soil. The performance testing concluded that the optimum ratio for fly ash with GBS is 3% fly ash + 6% GBS. Significant enhancement has been noted in the soils' unsoaked and soaked CBR values with the application of this optimal quantity. Alves et al. [3] evaluated that incorporating steel slag into the crushed limestone led to enhancements in both the mechanical properties and resistance aspects. Biradar et al. [5] indicated that the addition of steel slag and fly ash reduced consistency constraints and increased the CBR (California Bearing Ratio) value of the soil. Aldeeky and Al Hattamleh [1] stated that 20% FSSA (fine steel slag aggregate) additions reduce the plasticity index by 26.3% and free swell by 58.3% of the high plastic subgrade soil. Additionally, 20% FSSA additions enhance unconfined compressive strength, maximum dry density, and CBR by 100%, 6.9%, and 154%. Mohammed and Elsageer [9] showed that adding steel slag and lime improves the compaction behavior of stabilized sandy soil and enhances its density.

Muthukkumaran and Anusudha [10] indicated that adding a 12.5% mixture of (Cu slag and lime) to the clay soil resulted in a significant 30% improvement in dynamic shear modulus, a 56% drop in damping ratio, and a nearly 104% increase in resilient modulus. Zhang et al. [15] presented that steel slag (SL) utilization improved soil shear strength and dynamic modulus by increasing the internal friction angle based on static and dynamic properties. Alves et al.[2] examined laboratory slag–rubber mixture mechanical properties with CBR, monotonic, and cyclic triaxial testing. It was shown that slag–rubber mixtures can be durable and sturdy enough for transport infrastructure support layers if the rubber content is below 5% and the slag is milled to meet the grain size distribution ranges in the technical specifications of the cited countries.

Hasen and Abbas [16] conducted a study on the reinforcement of sandy soil with geogrid, explicitly focusing on three earthquakes' effects (Halabjah, Bolunun, and Ali Al-Gharbi) on a shaking table. Testing was conducted on specimens of sandy particles having a 70% density, both with and without support from geogrids. A total of five geogrid layers were used with a foundation measuring 100*100*30 mm, promoting a static load of 5.294 kN/m2. It was discovered that the dynamic force results in settlement, and a higher seismic acceleration of the earthquake causes more excellent settlement of the footings on sandy soil. If the acceleration of the earthquake is lower, the speed of settlement of the foundation will also be lower as the number of layers of geogrid increases.

During this study, a large model was employed to study the settlement properties of treated sandy soil with steel slag under seismic action (El Centro, Kobe). Steel slag was added to sandy soil with three percentages (3%, 6%, and 9%) and compacted with a relative density of 56%, and 77%. The study aims to reduce the settlement of circular foundation under earthquake load in sandy soil treated with steel slag.

2. Laboratory Work

2.1. Soil Properties

The soil used for the model tests was "Al-Ukhaidir" (Karbala) sands. The Sand was dry, crushed into small pieces, and separated using a sieve with a mesh size of #10 (2mm). Several tests were performed on Sand with two different relative densities, namely medium (Dr = 56%) and dense (Dr = 77%). The soil tests are conducted according to the parameters specified by ASTM and BS. The parameters obtained from the performed experiments and the traditional sand method are reported in Table 1.

Table 1: Physical and chemical properties and tests carried out on soils with the used standard.

Soil Property	Medium Sand	Dense Sand	Standard
Relative density, Dr (%)	56	77	
Max. dry unit weight, γd max (kN/m^3)	16.834		ASTM D4253 (2000)
Min. dry unit weight, γd min (kN/m^3)	14.06		ASTM D4254 (2000)
Dry unit weight, γd (kN/m^3)	15.33	16.1	
Total unit weight, γt (kN/m^3)	18.85	19.25	
Water content, Wc (%)	17	13	ASTM D2216 (2010)
Specific gravity, Gs	2.675		ASTM D854 (2014)
Sand, (%)	97		ASTM D422 (2007)
Silt, (%)	3		
D10, D30, D50, D60 (mm)	0.132, 0.333, 0.454, 0.511		
Coefficient of uniformity, Cu	3.871		
Coefficient of curvature, Cc	1.643		
Soil classification (USCS)*	Poorly-graded sand, (SP)		ASTM D2487 (2010)
Soil color	Pale yellow		
Friction angle, φ	36.8°	43.6°	ASTM D4767 (2011)
Cohesion, c (kN/m^2)	0	0	
pH	7.13		ASTM D4972 (2013)
SO_3, (%)	1.723		BS 1377-3 (1990)
Organic content, (%)	1.89		ASTM D2974 (2014)
Cl^{-1}, (%)	0.077		ASTM D1411 (2009)
$CaCO_3$, (%)	0.0		BS 1377-3 (1990)

2.2. Steel Slag

The waste came from steel manufacturing in the Bazian region of the Sulaymaniyah Governorate. The leftover material is generated as a secondary product of the iron Smelting process. The slag was further pulverized using a jaw crusher and then filtered through a 250-micron sieve (No.60). Slag's chemical makeup was similar to that of Portland cement; it included Silica, Magnesium oxide (MgO), calcium oxide (CaO) and Aluminum oxide (Al_2O_3), as shown in the Table 2; the specific weight for the slag was (3.38). figure 1 displays the ultimate configuration of steel slag following the grinding process and its passage through sieve No.60.

Table 2: The fundamental makeup of iron slag employed in the current investigation.

Chemical components	Percentages (%)
Ferric oxide (Fe_2o_3)	49.74
Calcium oxide (CaO)	20.52
Silica, amorphous (SiO_2)	14.53
Aluminum oxide (Al_2O_3)	5.55
Magnesium oxide (MgO)	3.92
Other	5.74

Fig 1. *Shows the steel slag.*

3. Design and Manufacture of a Shake Table

3.1. Components that make up a shake table include mechanical parts.

[17] investigated and developed a shaking table design with a steel structure measuring 600*1200*100 mm, screwed to the ground, and a cart base of 800*800*80 mm. Wheels connected to sliding tubes of steel move the cart's base. The exterior frame was on 10 mm rubber. It prevents device vibration and keeps the rubber cushion flush to the floor. figure 2 (a, b, c, d, and e) illustrates the shaking table's mechanical components. The 40-mm ball screw shaft is equipped with. To transform the motor's rotational motion into linear movement, the total length is 750 mm, with a route length of 620 mm. Two ball screw nut brackets secured the shaking table chassis. One bracket secured the drive rod, and another bracket held the rocking table frame. This allows the ball screw to move smoothly along the frame.

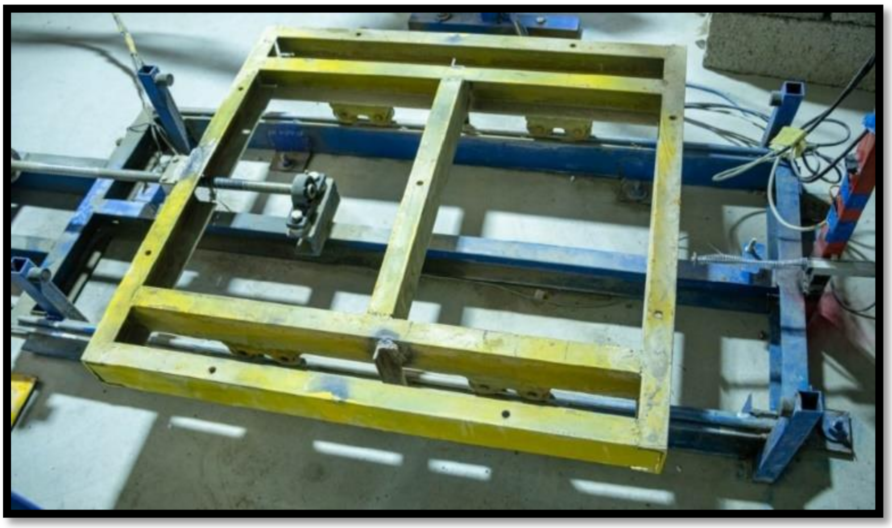

(a) Base shaking table.

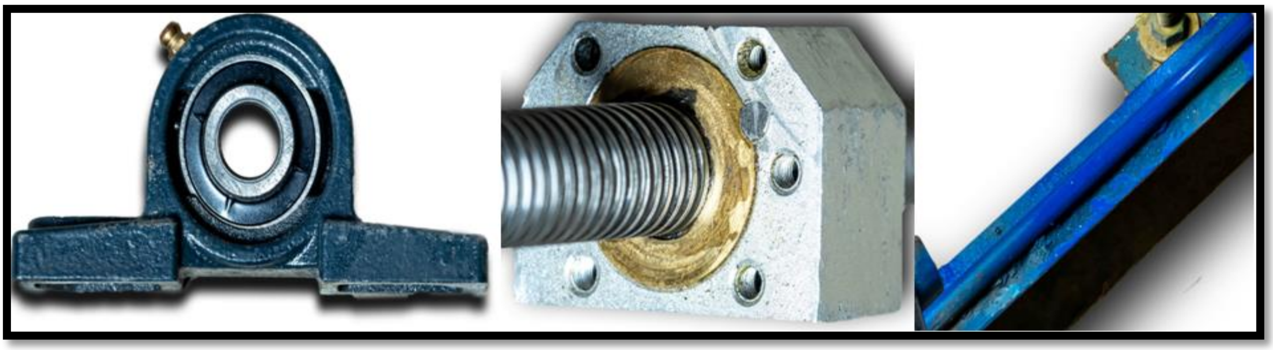

(b) First nut bracket. **(c)** Second nut bracket. **(d)** Sliding steel tubes.

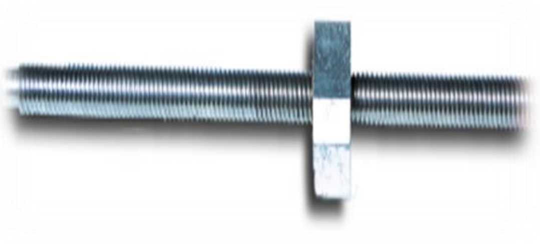

(e) Screw shaft.

Fig 2. *The mechanical components of a shaking table.*

3.2. Servo Motor and Drive

Servomotors (Electronic Commutation Delta AC Servo Motor) effectively control the path, velocity, and angular position. Vibrating position sensors power it. Simple interfaces for the Kollmorgen servo motor "AKM 73P-ACCNDA01" of the model number "AKD-P02407-NBEC-0000," three-phase electrical supply, and EtherCAT protocol connection were provided by the position indexer control module (movement tasks). figure 3 illustrates the servo motor and drive, while Table 3 lists product specs. The Arduino utilizes computer seismic information. The inverter moves the car by matching the shaker table's input wave.

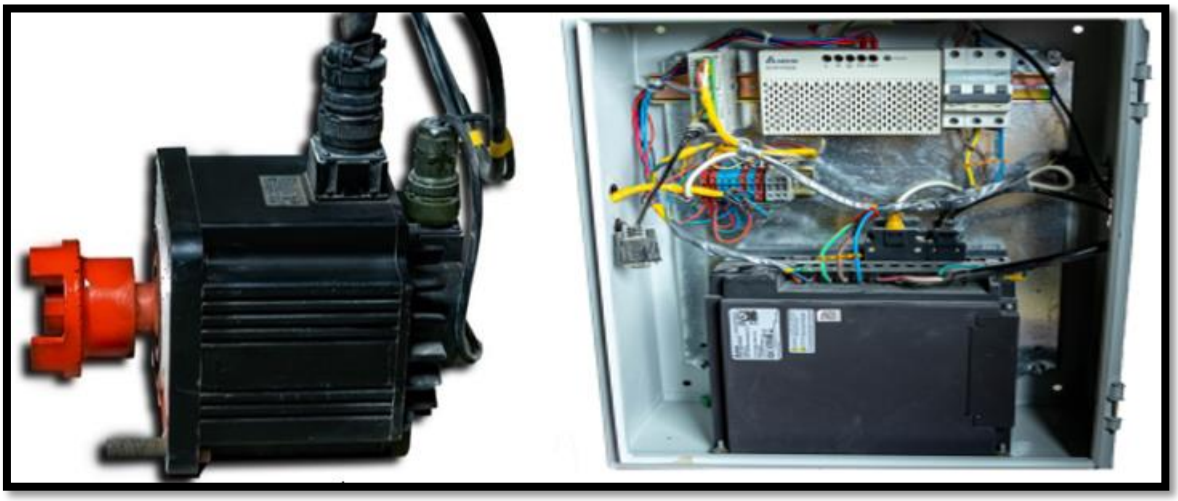

(a) Servo motor. *(b) Servo motor drive.*

Fig 3. *Servo motor and servo motor drive.*

Table 3: Servo motor specifications.

Item	Product ID	Name of the Series	Rated Voltage	Encoder Type	Motor Frame Size	Shaft Diameter	Rated Power Output	Net weight
Specifications	ECMA-L11830RS	A2	220V	incremental type, 20-bit	180x180mm	35mm	4500 W	18.5 kg

3.3. Methods

The Linear Variable Differential Transformer (LVDT) Sensor: It is estimating direct displacement with the linear changing differential inductor. With a standard output signal and a sealed electronic circuit that can function in moist and covered-dust conditions, the DC LVDT has excellent qualities. The device has a 20-millimeter hydraulic cylinder and stainless-steel casing. This test used three LVDT sensors to detect and control valve position and placement. Tables 4 list LVDT specifications. figure 4 show the 100mm LVDT dimensions and the ones used in this study.

Table 4: LVDT Sensor Specification.

Model	Supply voltage	Length	Measuring range	Output signal	Resolution	Operating Temp.
specifications	9-12VDC	346 mm	100mm	0-5v	≤0.1um, 16bit	-25℃ ~ +85℃

Fig 4. *LVDT Sensors.*

3.4. Execution of seismic data:

Precise seismic acceleration records were utilized. The settlement of circular footing was studied using natural acceleration histories from El Centro and Kobe to examine the impact of acceleration characteristics. The data for each earthquake is presented in Table 5 and Figure 5 shows the historical acceleration examples that were examined.

Table 5: Information of earthquake data.

Earthquake	El Centro	Kobe
Region:	California - USA	Japan
Date (UTC*):	1940-05-19 04:36:41	1995-01-16 20:46:52
Magnitude, (Mw):	6.9 Mw	6.9 Mw
Modified Mercalli Intensity, (MMI):	X- Extreme	VII- Very strong
Epicenter depth, (km):	8.8	17.9
Shake duration, (sec):	35	48
Station distance to epicenter, (km):	12.2	1.0
Sampling frequency, (Hz):	50	50
Acceleration direction:	N-S	N-S
Maximum acceleration, (g):	0.35	0.82
Station code:	ELC0A	KJMA
Reference:	www.strongmotiomcenter.org	www.strongmotiomcenter.org

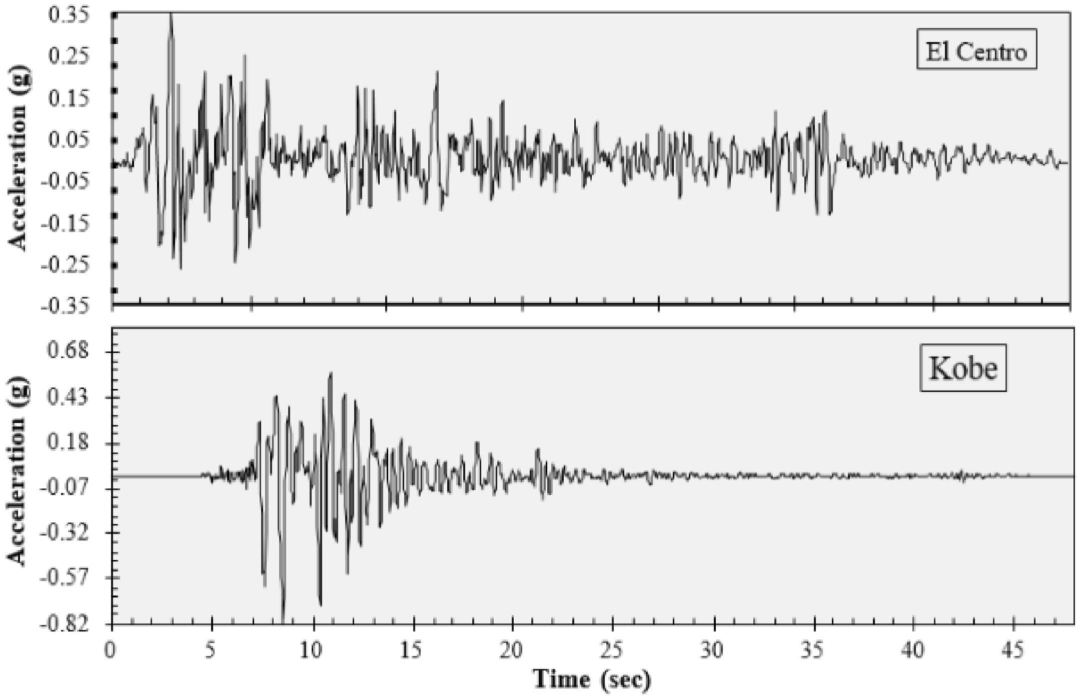

Fig. 5 *Acceleration history for the used earthquake.*

3.5. PC software for simulating earthquakes

The Earthquake Simulator uses LabVIEW 2020 Graphical code. The software performs inputs such as shaking acceleration, shaking, DAQ, data logging, analysis, and reporting. Programming this system requires LabVIEW. Reconfigurable input and output are included into the Data Logar real-time production control and data collecting system. Its reconfigurable I/O module architecture, programmable gates array (FPGA), and real-time controller make it dependable, strong, and high-performing for a variety of hardware tasks, including specialized timing and triggering, hardware algorithms, high-speed management, and signal processing. The Earthquake Simulator comprises two phases:

- Data Acquisition (DAQ).
- Reporting and Analysis of Data.

3.6. Flexible laminar shear box (FLSB)

[4]explored container pros and cons and model container requirements. Using flexible laminar containers, wave reflections from the final wall's lateral stiffness and stiff border were reduced. The soil-box system may nonetheless be regulated by the soil. The soil and foundation models in the FLSB are reliable. The fixed-side box borders are minimized by this box. When comparing models of soil behavior with side reflectance, laminae horizontal deformation lowers the border. FLSB end walls simulate the shear stiffness of soil models. The top twelve square steel laminae are fixed to rails so that the FLSB may move in a single direction. Steel-dimensional laminae are seen in Figure 6. The square frame is welded to a height of 600 mm and 50 mm for each lamina, measuring 600*600 mm on the inside and 700*700 mm outside. Between lamina, thin linear rail segments with balls bearing were fused.. These strips are 500 mm long, 43 mm broad, and 12.5 mm high. After the laminae were attached to a steel square plate base framework with an 800*800 mm outside diameter and 120 mm height, the FLSB was 720 mm tall. The pushing force was split by the top laminae weight's normal force.

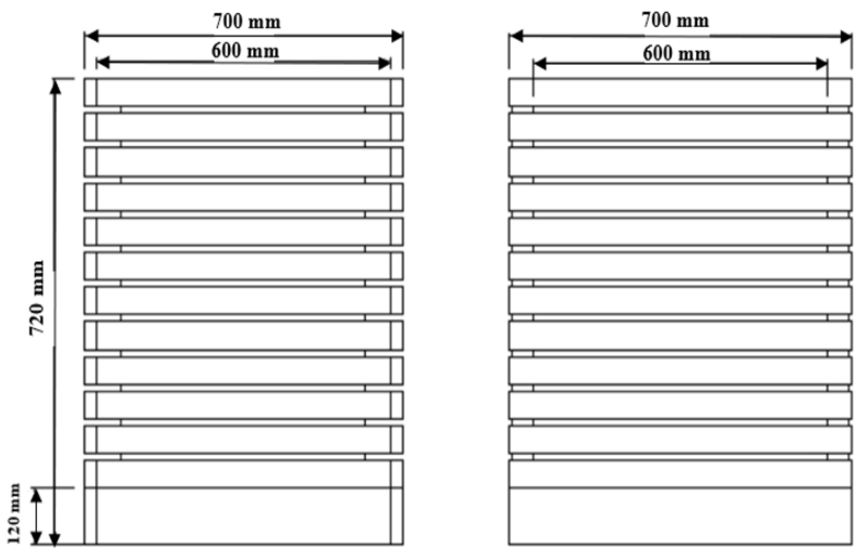

Fig. 6 *Flexible laminar shear box.*

3.7. Saturated System

A square network of pipes with a diameter of 0.5 inches (12.7 mm) was used for saturating the soil model. These pipes were enclosed in cloth to prevent clogging. The saturating system was positioned at the bottom of the laminar box behind a 120-mm-thick filter with coarse grains. This arrangement prevents the soil from being carried away by water during drainage, which occurs after the test when a water pump is employed.

3.8. Footing Model

The experimental work illustrated in figure 9 utilized a circular foundation constructed from a compact plastic block with a diameter (D_f) of 100 mm matching the dimensions of the full-scale model (1500 mm), and a thickness of 40 mm matching the dimensions of the full-scale model (600 mm). The block's bottom was coated with sandpaper to replicate the friction angle of saturated loose sand when in contact with plastic. Additionally, a fixed stress of 4.758 KN/m^2 was applied. Figure 7 displays the foundation model.

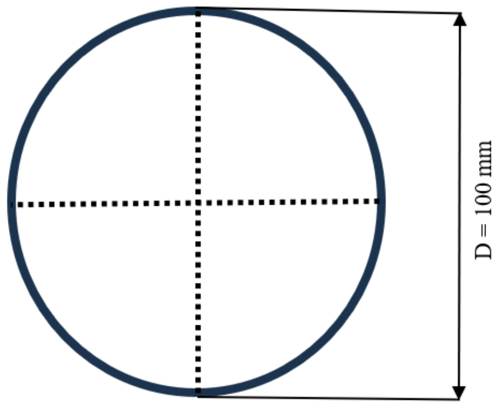

Fig. 7 The models of the footings (not drawn to scale).

4. Shake table testing program

A total of twenty-eight shaking table tests were conducted on two different sand densities, each with varying ratios of Steel Slag materials, with dry and saturated soil. These tests were carried out in reaction to two distant earthquakes that possessed seismic acceleration histories. The flowchart of the testing program is depicted in Figure 8.

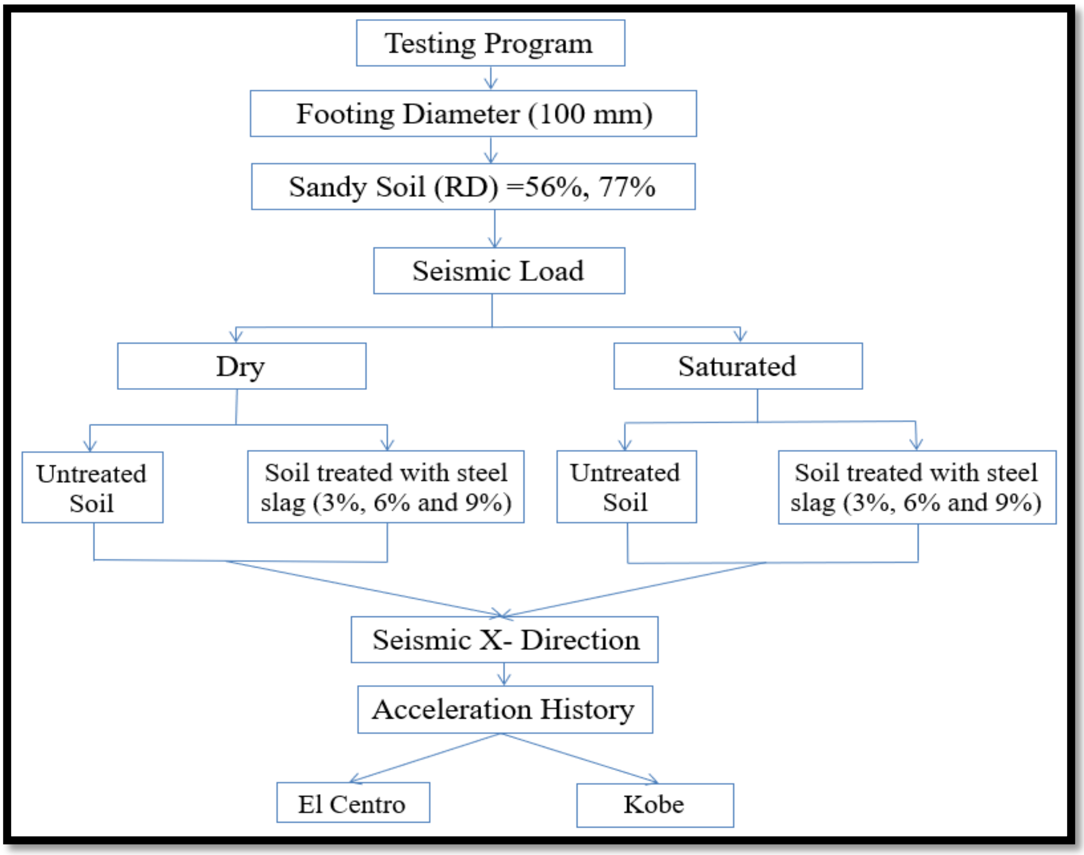

Fig. 8 The testing program.

5. Results and Discussion

This study presents the impact of applying steel slag (3%, 6%, and 9% to sandy soil) on the transmission of dynamic seismic stresses from the El Centro and Kobe earthquakes beneath a circular foundation. The foundation's settling due to these loads was analyzed. The evaluation process concentrated on the behavior of surface foundations, which represented the most hazardous condition. Additionally, it examined the effects of variables from two distinct earthquakes and two relative soil densities at varying steel slag mixing ratios under both dry and saturated soil conditions. figure 9 illustrates the settlement of the foundation due to induced seismic loads.

(a) Settlement during the test. **(b)** Settlement for treated soil.

Fig 9. *Settlement of foundation.*

Table 6 and Figures 10 and 11 illustrate the settlement behavior of the circular footing on sandy soil, mixed with steel slag at 3%, 6%, and 9% concentrations, at relative densities of 56% and 77%, under the influence of the El Centro earthquake. The settlement of the untreated soil was 0.163 Df (where Df represents the footing diameter in mm) and progressively diminished with the addition of steel slag, ultimately reaching 0.102 Df at a mixing ratio of 9% for a relative density of 56%. At a relative density of 77%, the settlement was 0.146 Df for untreated soil and decreased to 0.0886 Df at a mixing ratio of 9%. At a relative density of 56%, the percentages of settling that were seen were 18.4%, 26.38%, and 37.42%. At a relative density of 77%, they were 19.86%, 30.8%, and 39.31% for the three mixing ratios of 3%, 6%, and 9%. Consequently, the ratio of diminishing settlement is greater at a relative density of 77%.

Table 6: Foundation settlement influenced by the El Centro earthquake for the dry natural and treated sandy soil.

Case of soil	Settlement (mm) at Dr = 56%	The percentage of decrease in the settlement rate	Settlement (mm) at Dr = 77%	The percentage of decrease in the settlement rate
Untreated soil	0.163 D_f	-	0.146 D_f	-
Soil + 3% steel slag	0.133 D_f	18.4 %	0.117 D_f	19.86 %
Soil + 6% steel slag	0.12 D_f	26.38 %	0.101 D_f	30.8 %
Soil + 9% steel slag	0.102 D_f	37.42 %	0.0886 D_f	39.31 %

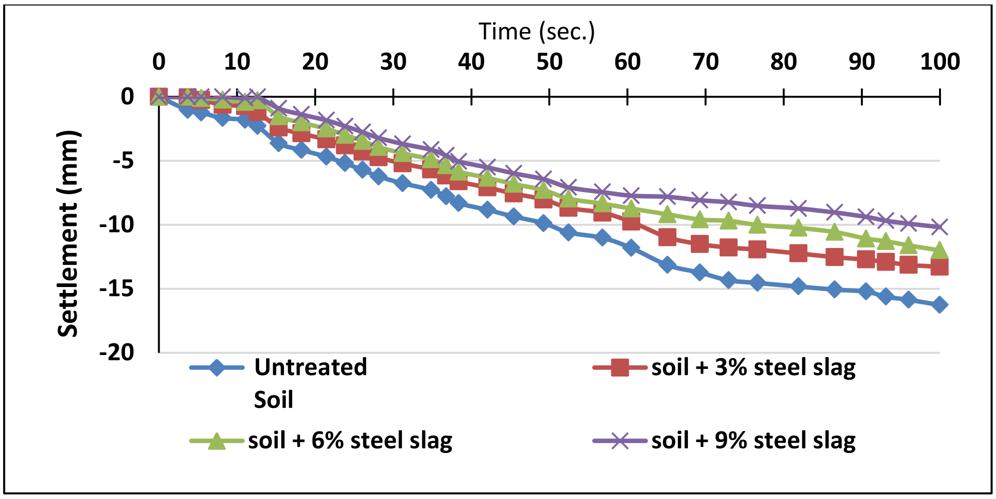

Fig. 10 Foundation settlement at Dr =56% with El Centro earthquake in dry natural and treated sandy soil.

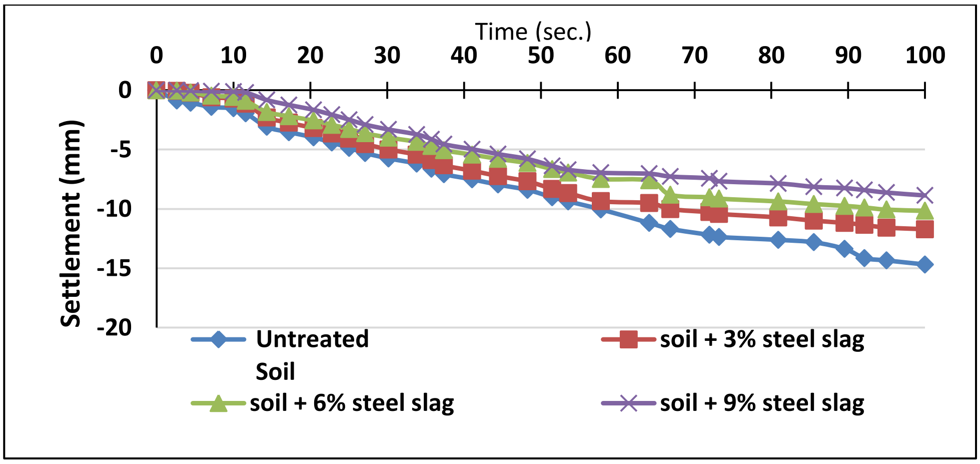

Fig. 11 Foundation settlement at Dr =77% with El Centro earthquake in dry natural and treated sandy soil.

The settlement behavior of the circular footing on sandy soil mixed with steel slag at proportions of 3%, 6%, and 9%, with relative densities of 56% and 77%, under the influence of the Kobe earthquake is illustrated in Table 7, Figures 12 and 13. The untreated soil exhibited a settlement of 0.233 Df, which diminished progressively with the introduction of steel slag, ultimately reaching 0.141 Df at a mixing rate of 9% for a relative density of 56%. At a relative density of 77%, the settlement was 0.198 Df for untreated soil, decreasing to 0.119 Df at a mixing ratio of 9%. At a relative density of 56%, the observed percentage of settlements decreased to 13%, 26.9%, and 36.77%, whereas at a relative density of 77%, they were 13.63%, 28.28%, and 39.89%, respectively. Consequently, the ratio of diminishing settlement is greater at a relative density of 77%.

Table 7: Foundation settlement influenced by the Kobe earthquake for the dry natural and treated sandy soil.

Case of soil	Settlement (mm) at Dr = 56%	The percentage of decrease in the settlement rate	Settlement (mm) at Dr = 77%	The percentage of decrease in the settlement rate
Untreated soil	$0.223D_f$	-	$0.198D_f$	-
Soil + 3% steel slag	$0.194D_f$	13%	$0.171D_f$	13.63%
Soil + 6% steel slag	$0.163D_f$	26.9%	$0.142D_f$	28.28%
Soil + 9% steel slag	$0.141D_f$	36.77%	$0.119D_f$	39.89%

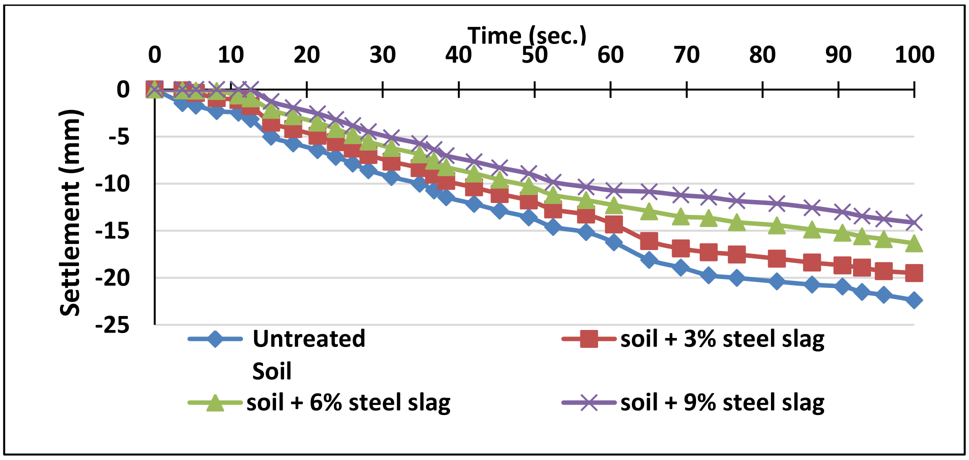

Fig. 12 *Foundation settlement at Dr =56% with Kobe Earthquake in in dry natural and treated sandy soil.*

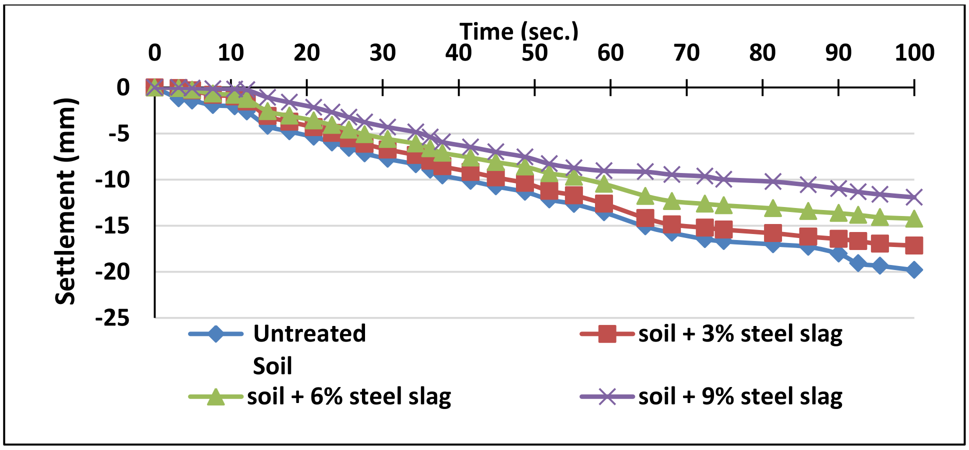

Fig. 13 *Foundation settlement at Dr =77% with Kobe Earthquake in dry natural and treated sandy soil.*

From Table 8, Figures 14 and 15, show the settlement behavior of the circular footing based on saturated granular soil at a relative density of 56 and 77%, for steel slag mixing ratios (3%, 6%, and 9%) under the influence of the El Centro earthquake.

The settling of the saturated untreated soil was 0.36 Df, which decreased to 0.259 Df at a 9% mixing rate of steel slag, corresponding to a relative density of 56%. At a relative density of 77%, the settlement was 0.342 Df for untreated soil and decreased to 0.233 Df at a mixing ratio of 9%. At a relative density of 56%, the observed percentage settlements dropped to 11.11%, 18.05%, and 28.05%, whereas at a relative density of 77%, they were 13.7%, 22.5%, and 31.87%, respectively.

Table 8: Foundation settlement influenced by the El-Centro earthquake for the saturated natural and treated sandy soil.

Case of soil	Settlement (mm) at Dr = 56%	The percentage of decrease in the settlement rate	Settlement (mm) at Dr = 77%	The percentage of decrease in the settlement rate
Untreated soil	0.36 D_f	-	0.342D_f	-
Soil + 3% steel slag	0.32 D_f	11.11%	0.295D_f	13.7%
Soil + 3% steel slag	0.295 D_f	18.05%	0.265D_f	22.51%
Soil + 3% steel slag	0.259 D_f	28.05%	0.233D_f	31.87%

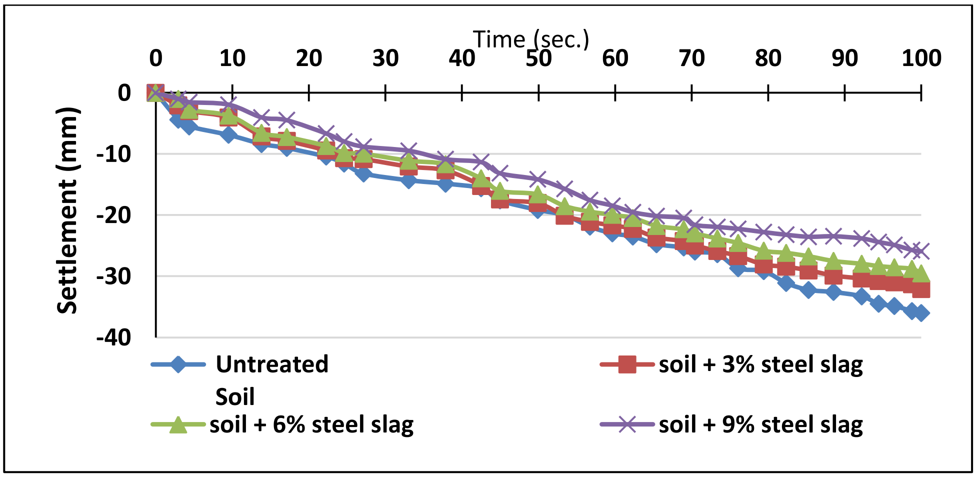

Fig. 14 *Foundation settlement at Dr =56% with El Centro Earthquake in saturated natural and treated sandy soil.*

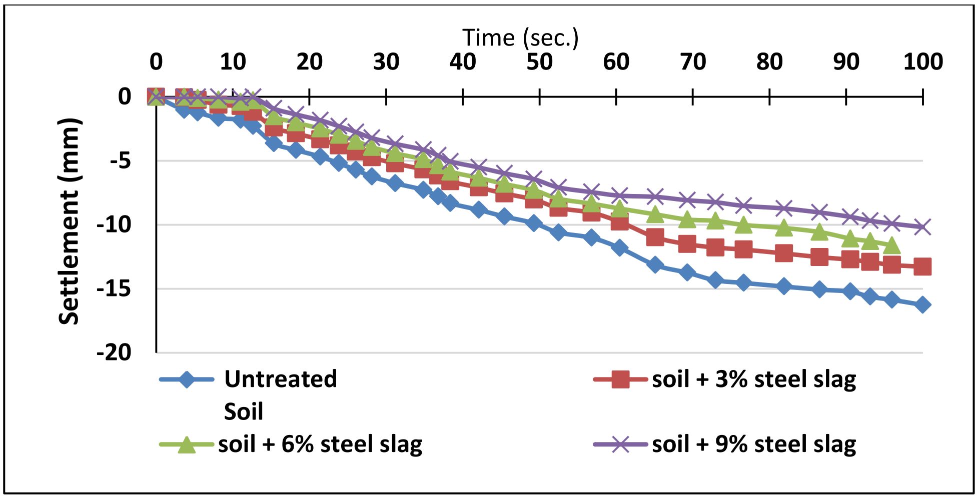

Fig. 15 *Foundation settlement at Dr =77% with El Centro Earthquake in saturated natural and treated sandy soil.*

The circular footing's settlement behavior on wet granular soil mixed with steel slag in amounts of 3%, 6%, and 9%, with relative densities of 56% and 77%, during the Kobe earthquake is shown in Table 9 and Figures 16 and 17. The untreated soil showed a settlement of 0.458 Df, which decreased to 0.353 Df with an increase in steel slag. This reduction occurred at a mixing rate of 9% and a relative density of 56%. At a relative density of 77%, the untreated soil's settlement measured 0.433 Df, which decreased to 0.324 Df at a mixing ratio of 9%. The settlement reduction rates seen were 7.64%, 16.15%, and 22.92% at a relative density of 56%. They were also 7.85%, 16.85%, and 25.17% at a relative density of 77% for the three mixing ratios of 3%, 6%, and 9%. Consequently, the ratio of settlement reduction is greater at a relative density of 77%.

Table 9: Foundation settlement influenced by the Kobe earthquake for the saturated natural and treated sandy soil.

Case of soil	**Settlement (mm) at Dr = 56%**	**The percentage of decrease in the settlement rate**	**Settlement (mm) at Dr = 77%**	**The percentage of decrease in the settlement rate**
Untreated soil	$0.458D_f$	-	$0.433D_f$	-
Soil + 3% steel slag	$0.423D_f$	7.64%	$0.399D_f$	7.85%
Soil + 6% steel slag	$0.384D_f$	16.15%	$0.36D_f$	16.85%
Soil + 9 % steel slag	$0.353D_f$	22.92%	$0.324D_f$	25.17%

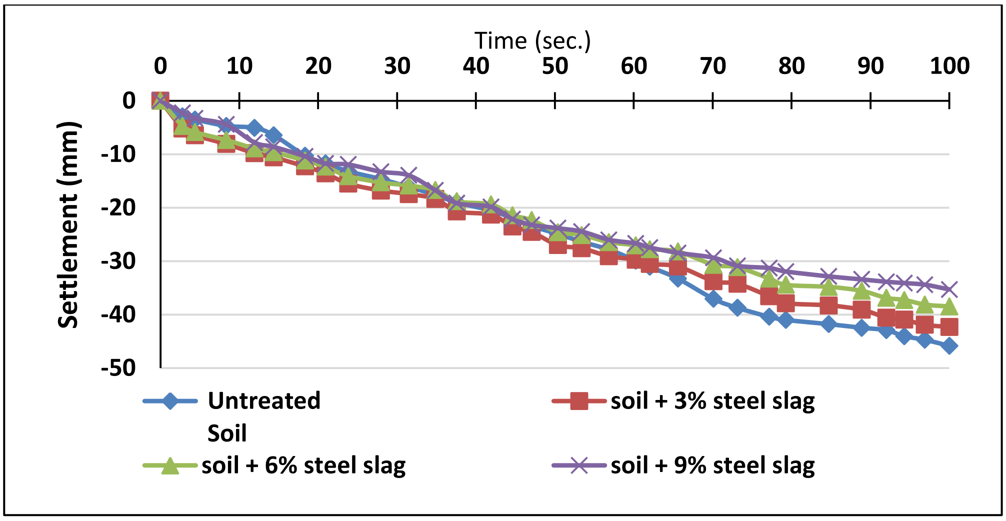

Fig. 16 Foundation settlement at Dr =56% with Kobe Earthquake in Saturated natural and treated sandy soil.

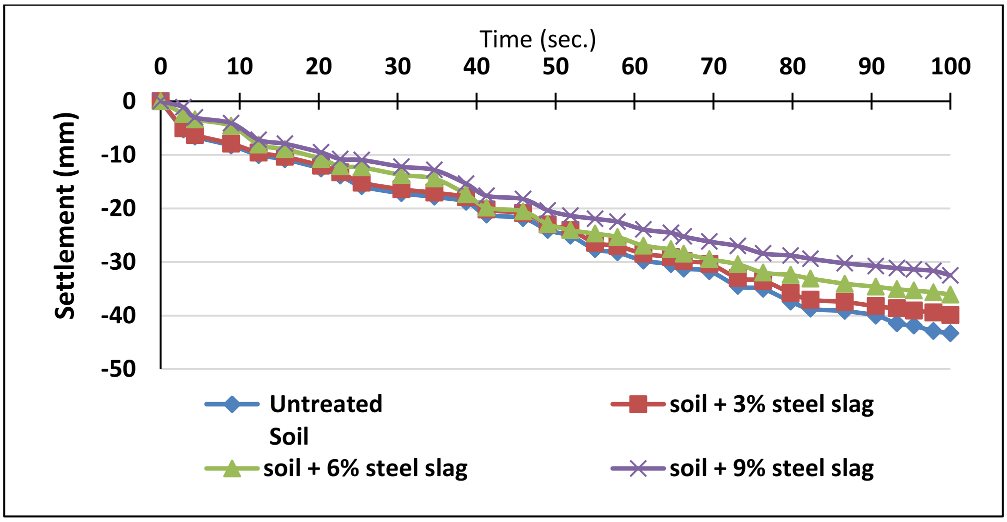

Fig. 17 Foundation settlement at Dr =77% with Kobe Earthquake in natural and treated sandy soil.

The results show that the acceleration of the earthquake causes soil accumulation and compression, which weake bonding between of the soil particles and causes foundation failure. The settlement may occur wholly or partially. The foundation's settling was found to diminish as the steel slag mixing ratio increased, continuing until the end of the earthquake duration.

When comparing the settlement results resulting from the El Centro and Kobe earthquakes, it could be noticed that the settlement in the Kobe earthquake was much greater than in the El Centro earthquake. This implies that the foundation will settle more quickly as the earthquake's acceleration rises and that the foundation will settle more slowly as the earthquake's acceleration decreases[16, 1, 18, 28, 31].

Furthermore, the foundation settlement diminishes as the steel slag mixing ratio increases in both dry and saturated conditions. In nearly all instances, the maximum stress differential ($\sigma1$-$\sigma3$) increases with the steel slag content. Only sandy soil significantly reduces the stress differential, but steel slag significantly increases it. The incorporation of steel slag will enhance the soil's strength. [24, 10].

6. Conclusions

The following results were obtained.

1. increasing the mixing ratios and relative density decreases the settlement of the foundation subjected to earthquake. As the mixing ratio increased to 9%, the settlement ratio decreased.
2. The settlement for the circular foundation decreases as the relative density of the sandy soil increases under the influence of the earthquake and for the dry and saturated state of the sandy soil.
3. The settlement of the circular foundation decreases as the mixing ratio with steel slag increases.
4. The settlement rate of the circular foundation in dry sandy soils exposed to earthquakes is approximately half the settlement rate in saturated soil. The settlement rate decrease in saturated soil is less than in dry soil.
5. In the dry state, the settlement decreased by (37.42% and 36.77%) at a relative density of 56% for the El Centro and Kobe respectively. At a relative density of 77%, the settlement rate decreased by (39.31% and 39.89%), respectively.
6. In the saturated state, the settlement decreased by (28.05% and 22.92%) at a relative density of 56% for the El Centro and Kobe respectively. At a relative density of 77%, the settlement rate decreased by (31.87% and 25.17%) for the El Centro and Kobe respectively.
7. The settlement for the saturated state was twice that for the dry state.

References

1- Aldeeky, H., & Al Hattamleh, O. (2017). Experimental study on the utilization of fine steel slag on stabilizing high plastic subgrade soil. *Advances in Civil Engineering*, *2017*.

2- Alves, R., Rios, S., Fortunato, E., Viana da Fonseca, A., & Guimarães Delgado, B. (2023). Mechanical Behaviour of Steel Slag–Rubber Mixtures: Laboratory Assessment. *Sustainability*, *15*(2), 1563.

3- Behiry, A. E. A. E. M. (2013). Evaluation of steel slag and crushed limestone mixtures as subbase material in flexible pavement. *Ain Shams Engineering Journal*, *4*(1), 43-53.

4- Bhattacharya, S., Lombardi, D., Dihoru, L., Dietz, M. S., Crewe, A. J., & Taylor, C. A. (2012). Model container design for soil-structure interaction studies. Role of seismic testing facilities in performance-based earthquake engineering, 135-158.

5- Biradar, K. B., Kumar, U. A., & Satyanarayana, D. P. (2014). Influence of steel slag and fly ash on strength properties of clayey soil: A comparative study. *International Journal of Engineering Trends and Technology (IJETT)-(14)(2). https://doi. org/10.14445/22315381/IJETT-V14P213*.

6- Horii, K., Tsutsumi, N., Kato, T., Kitano, Y., & Sugahara, K. (2015). Overview of iron/steel slag application and development of new utilization technologies. *Nippon Steel & Sumitomo Metal Technical Report*, *109*(109), 5-11.

7- Indraratna, B. (1996). Utilization of lime, slag and fly ash for improvement of a colluvial soil in New South Wales, Australia. *Geotechnical & Geological Engineering*, *14*, 169-191.

8- Liang, Y., Li, W., & Wang, X. (2013). Influence of water content on mechanical properties of improved clayey soil using steel slag. Geotechnical and Geological Engineering, 31, 83-91.
9- Mohammed, A. A., & Elsageer, M. A. A. (2018). The Effect of Adding Steel Slag and Lime on The Engineering Properties of a Sandy So.
10- Muthukkumaran, K., & Anusudha, V. (2020). Study on behavior of copper slag and lime–treated clay under static and dynamic loading. *Journal of Materials in Civil Engineering*, *32*(8), 04020230.
11- Ramaswamy, S. D., & Aziz, M. A. (1992). Some waste materials in road construction. In *Utilization of Waste Materials in Civil Engineering Construction* (pp. 153-165). ASCE.
12- Singh, G., Sangwan, S., & Usman, M. (2015). Experimental study of blast furnace slag concrete. *International Journal of Engineering Sciences and Research Technology Experimental*, *9655*(8), 475-480.
13- Wray, W. K., & Meyer, K. T. (2004). Expansive clay soil... a widespread and costly geohazard. *Geo-Strata—Geo Institute of ASCE*, *5*(4), 24.
14- Yadu, L., & Tripathi, R. K. (2013). Stabilization of soft soil with granulated blast furnace slag and fly ash. *International Journal of Research in Engineering and Technology*, *2*(2), 115-119.
15- Zhang, Y., Jiang, T., Li, S., & Wang, W. (2023). Engineering Properties and Environmental Impact of Soil Mixing with Steel Slag Applied in Subgrade. *Applied Sciences*, *13*(3), 1574.
16- Hasen N. A. and Abbas J. K. (2024). Experimental Study of Shallow Foundation Settlement Under Dynamic Load In Reinforced Sandy Soil. *Proceedings on Engineering Sciences*. 6(1), 171-178.
17- Hasen N. A. (2023). Effect of Dynamic Load on the Behavior of Shallow Footing Resting on Reinforced sandy Soil (Doctoral dissertation, Department of Civil Engineering, Tikrit University).
18- Shu, K.; Sasaki, K. Occurrence of steel converter slag and its high value-added conversion for environmental restoration in China: A review. J. Clean. Prod. 2022, 373, 133876.
19- Wang, X.; Li, X.; Yan, X.; Tu, C.; Yu, Z. Environmental risks for application of iron and steel slags in soils in China: A review. Pedosphere 2021, 31, 28–42.
20- Guo, J.; Bao, Y.; Wang, M. Steel slag in China: Treatment, recycling, and management. Waste Manag. 2018, 78, 318–330.
21- Shi, Y.; Chen, H.; Wang, J.; Feng, Q. Preliminary investigation on the pozzolanic activity of superfine steel slag. Constr. Build. Mater. 2015, 82, 227–234.
22- Wang, K.; Qian, C.; Wang, R. The properties and mechanism of microbial mineralized steel slag bricks. Constr. Build. Mater. 2016, 113, 815–823.
23- Wang, S.; Li, X.; Ren, K.; Liu, C. Experimental research on steel slag stabilized soil and its application in subgrade engineering. Geotech. Geol. Eng. 2020, 38, 4603–4615.
24- Li, W.; Lang, L.; Lin, Z.; Wang, Z.; Zhang, F. Characteristics of dry shrinkage and temperature shrinkage of cement-stabilized steel slag. Constr. Build. Mater. 2017, 134, 540–548.
25- Liu, J.; Yu, B.; Wang, Q. Application of steel slag in cement treated aggregate base course. J. Clean. Prod. 2020, 269, 121733.

26- Li, Q.; Li, B.; Li, X.; He, Z.; Zhang, P. Microstructure of pretreated steel slag and its influence on mechanical properties of cement stabilized mixture. Constr. Build. Mater. 2022, 317, 125799.
27- Gao, B.; Yang, C.; Zou, Y.; Wang, F.; Zhou, X.; Barbieri, D.M.; Wu, S. Compaction procedures and associated environmental impacts analysis for application of steel slag in road base layer. Sustainability 2021, 13, 4396.
28- Yildirim, I.Z.; Prezzi, M. Subgrade stabilisation mixtures with eaf steel slag: An experimental study followed by field implementation. Int. J. Pavement Eng. 2022, 23, 1754–1767.
29- Ma, Y.; Luo, Y.; Ma, H.; Zhou, X.; Luo, Z. Upcycling steel slag in producing eco-efficient iron-calcium phosphate cement. J. Clean. Prod. 2022, 371, 133688.
30- Tian, E.; Liu, Y.; Cheng, X.; Zeng, W. Characteristics of pavement cement concrete incorporating steel slag powder. Adv. Mater. Sci. Eng. 2022, 2022, 6360301.
31- Zhang, S.; Ghouleh, Z.; Mucci, A.; Bahn, O.; Provencal, R.; Shao, Y. Production of cleaner high-strength cementing material using steel slag under elevated-temperature carbonation. J. Clean. Prod. 2022, 342, 130948.